

# Data-driven Moving Horizon Estimation for Angular Velocity of Space Noncooperative Target in Eddy Current De-tumbling Mission

Xiyao Liu, *Student Member, IEEE*, Haitao Chang, *Member, IEEE*, Zhenyu Lu, *Member, IEEE*, Panfeng Huang, *Senior Member, IEEE*

**Abstract**—Angular velocity estimation is critical for eddy current de-tumbling of noncooperative space targets. However, unknown model of the noncooperative target and few observation data make the model-based estimation methods challenged. In this paper, a Data-driven Moving Horizon Estimation (Dd-MHE) method is proposed to estimate the angular velocity of the noncooperative target with de-tumbling torque. In this method, model-free state estimation of the angular velocity can be achieved using only one historical trajectory data that satisfies the rank condition. With local linear approximation, the Willems' fundamental lemma is extended to nonlinear autonomous systems, and the rank condition for the historical trajectory data is deduced. Then, a data-driven moving horizon estimation algorithm based on the M-step Lyapunov function is designed, and the time-discount robust stability of the algorithm is given. In order to illustrate the effectiveness of the proposed algorithm, experiments and simulations are performed to estimate the angular velocity in eddy current de-tumbling with only de-tumbling torque measurement.

**Index Terms**—Data-driven estimation, Moving horizon estimation, Angular velocity estimation, Robust stability.

## I. INTRODUCTION

THE angular velocity estimation of space noncooperative targets is critical for trajectory planning and control in autonomous spacecraft proximity operations [1]. Model-based estimation methods, like Kalman Filter [2] and Moving Horizon Estimation [3], have achieved great success and are widely used in noncooperative rendezvous [4], spacecraft relative navigation [5]. However, with the increasing complexity and uncertainty of space missions, it is not easy to accurately build the dynamic models of some situations, such as eddy current de-tumbling [6] and tethered space net robot [7]. It makes the model-based estimation method challenging to implement.

In recent years, data-driven methods have significantly been developed, such as learning-based data-driven [8], Koopman operator-based data-driven [9], and Willems' fundamen-

tal lemma-based data-driven [10]. The learning-based data-driven state estimation consists of different deep learning networks, hyperparameters, and their learning methods [11]. The learning-based data-driven state estimation methods [12], [13] are widely concerned in power systems and need abundant data to learn the model. The Koopman operator provides a path to represent nonlinear systems in a linear framework, which complements the classical and statistical perspectives on dynamic systems [14]. Surana *et al.* [15] first proposed a linear observer based on the Koopman operator for nonlinear systems and extended this method to the constrained state estimation problem [16], [17]. Guo *et al.* [18] combined the computational efficiency of Koopman state estimation and the generality of the kernel-embedding method through Random Fourier Features and verified the algorithm on a mobile robot.

The above methods require a big data set to obtain an accurate deep learning network or all the eigenvalues. However, in the mission of eddy current de-tumbling [6], [19] where experiments cannot be repeated, the data set is not abundant and only has historical data on a single trajectory. A data-driven method based on behavior theory, the Willems' fundamental lemma [20], is a viable scheme for the angular velocity estimation of the mission. The lemma states that for a controllable linear time-invariant system, any trajectory of the system can be determined from the corresponding input-output data as long as the historical input data satisfy the persistently exciting condition [21].

For state estimation based on this lemma, Adachi *et al.* [22] designed a data-driven observer based on matrix representation of dual system. Turan *et al.* [23] proposed a data-driven observer for unknown inputs. Wolff *et al.* [24] proposed a data-driven moving horizon estimation for linear time-invariant systems and gave the global exponential stability of the estimator. These methods are designed for linear systems or without disturbance. However, the angular velocity estimation in the eddy current de-tumbling mission is nonlinear and disturbed. Therefore, a new data-driven estimation method for the angular velocity estimation of eddy current de-tumbling mission is needed, which can be used for unknown nonlinear systems with disturbance and small data sets.

Motivated by the above, the paper proposes a data-driven moving horizon estimation algorithm that can estimate the noncooperative target's angular velocity with unknown model.

This research was supported by the National Natural Science Foundation of China (Grant No.62103337 and No.61725303).

X. Liu, H. Chang, and P. Huang are with the Research Center for Intelligent Robotics, School of Astronautics, Northwestern Polytechnical University, Xi'an 710072, China, E-mail: (liuxiyao@mail.nwpu.edu.cn; htchang@nwpu.edu.cn; pfhuang@nwpu.edu.cn); Z. Lu is with Bristol Robotics Laboratory and University of the West of England, Bristol, UK, E-mail: (Zhenyu.lu@uwe.ac.uk). (*Corresponding author: Haitao Chang.*)

Based on the local linear approximation, the algorithm can locally handle the state estimation problem of unknown nonlinear systems. In addition, the method can estimate the angular velocity of noncooperative targets under constraint conditions, and is proved to be time-discounted robust stable [25] under local linear approximation. The main contributions of this paper are as follows:

- 1) A novel data-driven method for angular velocity estimation of noncooperative targets is proposed, which is model-free and requires only a small amount of data. Unlike the learning-based method [13] and the Koopman-based method [18], this method is based on the Willems' fundamental lemma under the behavior theory, and only one historical trajectory data satisfying the rank condition is required for data-driven estimation.
- 2) A Dd-MHE algorithm is developed, which can be applied to nonlinear autonomous systems through local linear approximation. Compared with [22]–[24], this algorithm can deal with the state estimation of nonlinear systems, while ensuring time-discounted robust stability under constraint satisfaction and disturbances. In addition, a pole placement method is provided for unknown systems, which gives lower bounds for the parameters that guarantee the stability of Dd-MHE.

The paper is structured as follows: the eddy current de-tumbling dynamics model is presented, and an extended Willems' fundamental lemma to autonomous systems is given in Section II. The data-driven moving horizon estimation algorithm and its time-discounted robust stability are given in Section III. The effectiveness of the proposed method is illustrated in Section IV with eddy current de-tumbling angular velocity estimation experiments and simulations.

*Notation:*  $\mathbf{I}_n$  represents  $n \times n$ -dimensional identity matrix,  $\otimes$  denotes the Kronecker product.  $\mathbf{1}_n$  represents an  $n$ -dimensional column vector with all entries equal to 1.  $\mathbf{0}$  denotes a matrix with corresponding dimensions and all entries equal to 0. The set of integers is expressed as  $\mathbb{I}$ , and the set of integers greater than or equal to  $a$  or between  $a$  and  $b$  are expressed as  $\mathbb{I}_{\geq a}$  and  $\mathbb{I}_{[a,b]}$  respectively. The maximal eigenvalues of matrix  $\mathbf{P}$  are denoted by  $\lambda_{max}(\mathbf{P})$ . A data sequence  $\mathbf{u}_{[i,j]}$  is a column vector with  $\mathbf{u}_{[i,j]} = [\mathbf{u}(i)^\top \ \mathbf{u}(i+1)^\top \ \cdots \ \mathbf{u}(j)^\top]^\top$ . For any matrix  $\mathbf{A}$ ,  $\mathbf{A}^\dagger$  denotes the pseudoinverse of  $\mathbf{A}$ . For any vector  $\mathbf{a} = [a_1 \ a_2 \ a_3]^\top$ ,  $(\cdot)^\times$  denotes the skew-symmetric matrix as follows:

$$\mathbf{a}^\times = \begin{bmatrix} 0 & -a_3 & a_2 \\ a_3 & 0 & -a_1 \\ -a_2 & a_1 & 0 \end{bmatrix}. \quad (1)$$

The Hankel matrix is given by:

*Definition 1:* The Hankel matrix  $\mathbf{H}_k(\mathbf{u}_{[i,j]})$  with depth  $k \in \mathbb{I}_{\geq 1}$  of any vector sequence  $\mathbf{u}_{[i,j]}$  is defined as

$$\mathbf{H}_k(\mathbf{u}_{[i,j]}) = \begin{bmatrix} \mathbf{u}(i) & \mathbf{u}(i+1) & \cdots & \mathbf{u}(j-k+1) \\ \mathbf{u}(i+1) & \mathbf{u}(i+2) & \cdots & \mathbf{u}(j-k+2) \\ \vdots & \vdots & \ddots & \vdots \\ \mathbf{u}(i+k-1) & \mathbf{u}(i+k) & \cdots & \mathbf{u}(j) \end{bmatrix}.$$

## II. PROBLEM SETUP AND PRELIMINARIES

In this section, we present and linearize the target's attitude dynamics model in the eddy current de-tumbling according to [6] and then extend Willems' fundamental lemma to linear autonomous systems with offsets in conjunction with [26].

### A. Attitude dynamics model in eddy current de-tumbling

According to [6], the attitude dynamics model of the unknown target in eddy current de-tumbling is

$$\mathbf{J}_t \dot{\boldsymbol{\omega}}_t + \boldsymbol{\omega}_t^\times \mathbf{J}_t \boldsymbol{\omega}_t = \boldsymbol{\tau}_t(\boldsymbol{\omega}_t), \quad (2)$$

where  $\mathbf{J}_t$  denotes the inertia tensor of the target,  $\boldsymbol{\omega}_t$  is the target's angular velocity,  $\boldsymbol{\tau}_t(\boldsymbol{\omega}_t)$  denotes the eddy current de-tumbling torque.

Since the target is unknown, the parameter  $\mathbf{J}_t$  and function  $\boldsymbol{\tau}_t(\boldsymbol{\omega}_t)$  in the above equation are not available. Therefore, the data-driven method is needed to estimate the target's angular velocity  $\boldsymbol{\omega}_t$ . The measured output is the eddy current de-tumbling torque on the chaser given as

$$\mathbf{y} = \boldsymbol{\tau}_c(\boldsymbol{\omega}_t). \quad (3)$$

Similarly,  $\boldsymbol{\tau}_c(\boldsymbol{\omega}_t)$  is a function of  $\boldsymbol{\omega}_t$  and is also not available. Note that one can obtain approximate equations for  $\boldsymbol{\tau}_t(\boldsymbol{\omega}_t)$  and  $\boldsymbol{\tau}_c(\boldsymbol{\omega}_t)$  by (6) and (9) in [19]. However, since the target is completely unknown, the parameters in these equations are also not available. Therefore, for the sake of brevity, we directly consider  $\boldsymbol{\tau}_t(\boldsymbol{\omega}_t)$  and  $\boldsymbol{\tau}_c(\boldsymbol{\omega}_t)$  as unknown functions.

Combining (2)-(3) and the forward-Euler method, one can directly deduce the following standard nonlinear discrete-time state space model:

$$\mathbf{x}(t+1) = \mathbf{f}(\mathbf{x}(t)), \mathbf{y}(t) = \mathbf{h}(\mathbf{x}(t)), \quad (4)$$

where  $\mathbf{x} = \boldsymbol{\omega}_t$  denotes the state, the discrete-time state function  $\mathbf{f}(\mathbf{x}(t)) = \mathbf{x}(t) + T_s \mathbf{J}_t^{-1} (\boldsymbol{\tau}_t(\mathbf{x}) - \mathbf{x}_t^\times \mathbf{J}_t \mathbf{x}_t)$ ,  $T_s$  is the sample interval, and the output function  $\mathbf{h}(\mathbf{x}(t)) = \boldsymbol{\tau}_c(\mathbf{x}(t))$ .

In the following content, we need the linearization model of (4). Thus, we define the linear autonomous system with offsets resulting from the linearization of (4) at point  $\tilde{\mathbf{x}}$  as

$$\begin{aligned} \mathbf{x}(t+1) &= \mathbf{A}_{\tilde{\mathbf{x}}} \mathbf{x}(t) + \mathbf{e}_{\tilde{\mathbf{x}}} + \mathbf{w}(t), \\ \mathbf{y}(t) &= \mathbf{C}_{\tilde{\mathbf{x}}} \mathbf{x}(t) + \mathbf{r}_{\tilde{\mathbf{x}}} + \mathbf{v}(t), \end{aligned} \quad (5)$$

where  $\mathbf{A}_{\tilde{\mathbf{x}}} = \left. \frac{\partial \mathbf{f}}{\partial \mathbf{x}} \right|_{\tilde{\mathbf{x}}}$ ,  $\mathbf{e}_{\tilde{\mathbf{x}}} = \mathbf{f}(\tilde{\mathbf{x}}) - \mathbf{A}_{\tilde{\mathbf{x}}} \tilde{\mathbf{x}}$ ,  $\mathbf{C}_{\tilde{\mathbf{x}}} = \left. \frac{\partial \mathbf{h}}{\partial \mathbf{x}} \right|_{\tilde{\mathbf{x}}}$ ,  $\mathbf{r}_{\tilde{\mathbf{x}}} = \mathbf{h}(\tilde{\mathbf{x}}) - \mathbf{C}_{\tilde{\mathbf{x}}} \tilde{\mathbf{x}}$ , and  $\mathbf{w}(t) = \mathbf{f}(\mathbf{x}(t)) - \mathbf{A}_{\tilde{\mathbf{x}}} \mathbf{x}(t) - \mathbf{e}_{\tilde{\mathbf{x}}}$  is the state function linearization error,  $\mathbf{v}(t) = \mathbf{h}(\mathbf{x}(t)) - \mathbf{C}_{\tilde{\mathbf{x}}} \mathbf{x}(t) - \mathbf{r}_{\tilde{\mathbf{x}}}$  is the output function linearization error. Note that  $\mathbf{A}_{\tilde{\mathbf{x}}}$ ,  $\mathbf{e}_{\tilde{\mathbf{x}}}$ ,  $\mathbf{C}_{\tilde{\mathbf{x}}}$  and  $\mathbf{r}_{\tilde{\mathbf{x}}}$  in (5) are unknown, and  $\mathbf{w}(t)$  and  $\mathbf{v}(t)$  can be regarded as process disturbance and measurement noise respectively.

### B. Extended Willems' fundamental lemma

To derive the data-driven method used in this paper, we extend the Willems' fundamental lemma [26] to the linear autonomous system with offsets.

*Lemma 1:* For a linear autonomous system with offsets:

$$\begin{aligned} \mathbf{x}(t+1) &= \mathbf{A}\mathbf{x}(t) + \mathbf{e}_o, \\ \mathbf{y}(t) &= \mathbf{C}\mathbf{x}(t) + \mathbf{r}_o, \end{aligned} \quad (6)$$

where  $\mathbf{e}_o$  and  $\mathbf{r}_o$  denote the offsets of the state equation and the output equation, respectively. Suppose one data sequence  $\{\mathbf{x}_{[0,T]}, \mathbf{y}_{[0,T-1]}\}$  is a trajectory of (6), and satisfies the rank condition as

$$\text{rank} \left( \begin{bmatrix} \mathbf{H}_1(\mathbf{x}_{[0,T-L]}) \\ \mathbf{1}_{T-L+1}^\top \end{bmatrix} \right) = n + 1, \quad (7)$$

where  $n$  is the dimension of the system state  $\mathbf{x}$ , and the data length  $T$  satisfies that  $T \geq L + n$ . Then, the other data sequence  $\{\mathbf{x}'_{[0,L]}, \mathbf{y}'_{[0,L-1]}\}$  is a trajectory of the system (6), if and only if there exists  $\boldsymbol{\alpha} \in \mathbb{R}^{T-L+1}$  such that

$$\begin{bmatrix} \mathbf{H}_{L+1}(\mathbf{x}_{[0,T]}) \\ \mathbf{H}_L(\mathbf{y}_{[0,T-1]}) \\ \mathbf{1}_{T-L+1}^\top \end{bmatrix} \boldsymbol{\alpha} = \begin{bmatrix} \mathbf{x}'_{[0,L]} \\ \mathbf{y}'_{[0,L-1]} \\ 1 \end{bmatrix}. \quad (8)$$

*Proof: Proof of “if”:*

Before starting the proof, we define the following matrix:

$$\begin{aligned} \Phi_K &= [\mathbf{I}_n^\top \quad \mathbf{A}^\top \quad \dots^\top \quad (\mathbf{A}^{K-1})^\top]^\top, \\ \Gamma_K &= [\mathbf{C}^\top \quad (\mathbf{C}\mathbf{A})^\top \quad \dots \quad (\mathbf{C}\mathbf{A}^{K-1})^\top]^\top, \\ \Psi_K &= [\mathbf{0}^\top \quad \mathbf{I}_n^\top \quad \dots \quad (\sum_{i=0}^{K-2} \mathbf{A}^i)^\top]^\top, \\ \Pi_K &= [\mathbf{0}^\top \quad \mathbf{C}^\top \quad \dots \quad (\mathbf{C}\sum_{i=0}^{K-2} \mathbf{A}^i)^\top]^\top. \end{aligned} \quad (9)$$

Since  $\{\mathbf{x}_{[0,T]}, \mathbf{y}_{[0,T-1]}\}$  is a trajectory of the system (6), the following equation can be derived as

$$\begin{bmatrix} \mathbf{H}_{L+1}(\mathbf{x}_{[0,T]}) \\ \mathbf{H}_L(\mathbf{y}_{[0,T-1]}) \end{bmatrix} = \begin{bmatrix} \Phi_{L+1} \\ \Gamma_L \end{bmatrix} \mathbf{x}_L + \begin{bmatrix} \Psi_{L+1} \\ \Pi_L \end{bmatrix} \mathbf{e}_L + \begin{bmatrix} \mathbf{0} \\ \mathbf{I}_{p,L} \end{bmatrix} \mathbf{r}_L, \quad (10)$$

where  $\mathbf{x}_L = \mathbf{H}_1(\mathbf{x}_{[0,T-L]})$ ,  $\mathbf{e}_L = \mathbf{1}_{T-L+1}^\top \otimes \mathbf{e}_o$ ,  $\mathbf{r}_L = \mathbf{1}_{T-L+1}^\top \otimes \mathbf{r}_o$ ,  $\mathbf{I}_{p,L} = \mathbf{I}_p \otimes \mathbf{1}_L$ .

By substituting (10) into (8), one can obtain

$$\begin{aligned} \begin{bmatrix} \mathbf{x}'_{[0,L]} \\ \mathbf{y}'_{[0,L-1]} \end{bmatrix} &= \begin{bmatrix} \Phi_{L+1} \\ \Gamma_L \end{bmatrix} \mathbf{x}_L \boldsymbol{\alpha} + \begin{bmatrix} \Psi_{L+1} \\ \Pi_L \end{bmatrix} \mathbf{e}_L \boldsymbol{\alpha} + \begin{bmatrix} \mathbf{0} \\ \mathbf{I}_{p,L} \end{bmatrix} \mathbf{r}_L \boldsymbol{\alpha} \\ &= \begin{bmatrix} \Phi_{L+1} \\ \Gamma_L \end{bmatrix} \mathbf{x}_L \boldsymbol{\alpha} + \begin{bmatrix} \Psi_{L+1} \\ \Pi_L \end{bmatrix} \mathbf{e}_o + \begin{bmatrix} \mathbf{0} \\ \mathbf{I}_{p,L} \end{bmatrix} \mathbf{r}_o. \end{aligned} \quad (11)$$

In the above derivation,  $\mathbf{1}_{T-L+1}^\top \boldsymbol{\alpha} = 1$  is adopted to make  $\mathbf{e}_L \boldsymbol{\alpha} = \mathbf{e}_o$  and  $\mathbf{r}_L \boldsymbol{\alpha} = \mathbf{r}_o$ .

Equation (7) directly derives that  $\mathbf{x}_L = \mathbf{H}_1(\mathbf{x}_{[0,T-L]})$  has rank  $n$ . Thus, (11) means that  $\{\mathbf{x}'_{[0,L]}, \mathbf{y}'_{[0,L-1]}\}$  is a trajectory of the system (6) with initial condition  $\mathbf{x}'(0) := \mathbf{H}_1(\mathbf{x}_{[0,T-L]}) \boldsymbol{\alpha}$ .

**Proof of “Only if”:**

Since  $\mathbf{H}_1(\mathbf{x}_{[0,T-L]})$  has rank  $n$ , it implies the existence of a vector  $\boldsymbol{\alpha} \in \mathbb{R}^{T-L+1}$  such that

$$\begin{bmatrix} \mathbf{H}_1(\mathbf{x}_{[0,T-L]}) \\ \mathbf{1}_{T-L+1}^\top \end{bmatrix} \boldsymbol{\alpha} = \begin{bmatrix} \mathbf{x}'(0) \\ 1 \end{bmatrix}. \quad (12)$$

Considering that  $\{\mathbf{x}'_{[0,L]}, \mathbf{y}'_{[0,L-1]}\}$  is a trajectory of system (6), the following derivation is available:

$$\begin{aligned} \begin{bmatrix} \mathbf{x}'_{[0,L]} \\ \mathbf{y}'_{[0,L-1]} \end{bmatrix} &= \begin{bmatrix} \Phi_{L+1} \\ \Gamma_L \end{bmatrix} \mathbf{x}'(0) + \begin{bmatrix} \Psi_{L+1} \\ \Pi_L \end{bmatrix} \mathbf{e}_o + \begin{bmatrix} \mathbf{0} \\ \mathbf{I}_{p,L} \end{bmatrix} \mathbf{r}_o \\ &\stackrel{(11)}{=} \begin{bmatrix} \Phi_{L+1} \\ \Gamma_L \end{bmatrix} \mathbf{x}_L \boldsymbol{\alpha} + \begin{bmatrix} \Psi_{L+1} \\ \Pi_L \end{bmatrix} \mathbf{e}_L \boldsymbol{\alpha} + \begin{bmatrix} \mathbf{0} \\ \mathbf{I}_{p,L} \end{bmatrix} \mathbf{r}_L \boldsymbol{\alpha} \\ &\stackrel{(10)}{=} \begin{bmatrix} \mathbf{H}_{L+1}(\mathbf{x}_{[0,T]}) \\ \mathbf{H}_L(\mathbf{y}_{[0,T-1]}) \end{bmatrix} \boldsymbol{\alpha}. \end{aligned} \quad (13)$$

Thereby, the proof of *Lemma 1* is completed.  $\blacksquare$

### III. DATA-DRIVEN MHE AND ROBUST STABILITY

In this section, we construct the robust data-driven Moving Horizon Estimation (MHE) optimization problem for linear autonomous systems with offsets based on the historical state/output trajectory and provide the **Algorithm 1**. Subsequently, we give the robust stability of **Algorithm 1** with the  $M$ -step Lyapunov function [27].

#### A. Data-driven MHE Algorithm

As stated in *Lemma 1* and Ref. [24], noise-free system state/output historical data is required to realize data-driven estimation. In eddy current de-tumbling, the historical state data can be obtained by visual-based systems such as Light Detection And Ranging (LIDAR) sensors, monocular and stereo cameras, etc [28]. In this paper, the historical data is defined as  $\{\mathbf{x}_{[-T,0]}, \mathbf{y}_{[-T,-1]}\}$ .

At time  $t \in \mathbb{I}_{\geq 1}$ , the proposed Data-driven MHE (Dd-MHE) optimization problem with horizon length  $M_t = \min\{t, M\}$  and  $M \in \mathbb{I}_{\geq 1}$  is

$$\begin{aligned} &\min_{\hat{\mathbf{x}}(\cdot|t), \boldsymbol{\alpha}(t), \hat{\mathbf{v}}(\cdot|t)} J_L(\hat{\mathbf{x}}(t - M_t|t), \hat{\mathbf{v}}(\cdot|t), t) \\ \text{s.t.} &\begin{bmatrix} \mathbf{H}_{M_t}(\mathbf{y}_{[-T,-1]}) \\ \mathbf{H}_{M_t+1}(\mathbf{x}_{[-T,0]}) \\ \mathbf{1}_{T-M_t+1}^\top \end{bmatrix} \boldsymbol{\alpha}(t) = \begin{bmatrix} \mathbf{y}_{[t-M_t,t-1]} - \hat{\mathbf{v}}_{[-M_t,-1]}(t) \\ \hat{\mathbf{x}}_{[-M_t,0]}(t) \\ 1 \end{bmatrix}, \end{aligned} \quad (14a)$$

$$\hat{\mathbf{x}}(j|t) \in \mathbb{X}, j \in \mathbb{I}_{[t-M_t,t]}, \quad (14b)$$

$$\hat{\mathbf{v}}(j|t) \in \mathbb{V}, j \in \mathbb{I}_{[t-M_t,t-1]}, \quad (14c)$$

where the cost function of this optimization problem is

$$\begin{aligned} J_L(\hat{\mathbf{x}}(t - M_t|t), \hat{\mathbf{v}}(\cdot|t), t) &= 2\rho^{M_t} \|\hat{\mathbf{x}}(t - M_t|t) - \bar{\mathbf{x}}(t - M_t)\|^2 \\ &\quad + \sum_{j=1}^{M_t} \rho^{j-1} \mu \|\hat{\mathbf{v}}(t - j|t)\|^2, \end{aligned} \quad (15)$$

and  $\hat{\mathbf{x}}(\cdot|t) = \{\hat{\mathbf{x}}(j|t)\}_{j=t-M_t}^{j=t}$ ,  $\hat{\mathbf{v}}(\cdot|t) = \{\hat{\mathbf{v}}(j|t)\}_{j=t-M_t}^{j=t-1}$  denote a sequence of  $M_t$  optimized state and noise estimates, respectively.  $\hat{\mathbf{x}}_{[-M_t,0]}(t) = [\hat{\mathbf{x}}(t - M_t|t)^\top, \dots, \hat{\mathbf{x}}(t|t)^\top]^\top$ , and  $\hat{\mathbf{v}}_{[-M_t,-1]}(t) = [\hat{\mathbf{v}}(t - M_t|t)^\top, \dots, \hat{\mathbf{v}}(t - 1|t)^\top]^\top$ .  $\mathbf{y}_{[t-M_t,t-1]}$  denotes the measurement output sequence at time interval  $[t - M_t, t - 1]$ .  $\mathbb{X}$  and  $\mathbb{V}$  are state and noise constraint sets, respectively, if given. The parameters  $\rho$  and  $\mu$  are set to ensure robust stability, which will be described in detail in the subsection III-B, and the horizon length  $M$  is limited to satisfying the inequality (31).

**Algorithm 1:** Dd-MHE for the system (5)

---

**Data Collection:** Collect historical data  $\{\mathbf{x}_{[-T,0]}, \mathbf{y}_{[-T,-1]}\}$  through sensors and ensure that the data satisfy the rank condition (7).

**Data Preprocessing:** Execute **Algorithm 2** and obtain  $\rho_0$  and  $\mu_0$ ; Given parameters  $\rho \in (\rho_0, 1)$ ,  $\mu > \mu_0$  and  $M$  that satisfies (31); Given the constraint sets  $\mathbb{X}$  and  $\mathbb{V}$ , and the priori estimate state  $\bar{\mathbf{x}}(0)$  of (14); Given the final time  $T_f$ .

**State Estimation:**

```

for  $t \leq T_f$  do
  if  $t \leq M$  then
    Create the optimization problem (14) with
       $M_t = t$ ;
    Let  $\bar{\mathbf{x}}(t - M_t) = \bar{\mathbf{x}}(0)$  and given the
      measurement output  $\mathbf{y}_{[t-M_t, t-1]}$  to (14);
    Solve (14) and obtain  $\hat{\mathbf{x}}^*(t|t)$ ;
  end
  if  $M < t \leq T_f$  then
    Let  $\bar{\mathbf{x}}(t - M_t) = \hat{\mathbf{x}}(t - M_t)$  and given the
      measurement output  $\mathbf{y}_{[t-M_t, t-1]}$  to (14);
    Solve (14) and obtain  $\hat{\mathbf{x}}^*(t|t)$ ;
  end
   $\hat{\mathbf{x}}(t) = \hat{\mathbf{x}}^*(t|t)$ ;
end

```

---

Therefore, we give the following Dd-MHE algorithm for the system (5), as shown in **Algorithm 1**.

*Remark 1:* It is worth noting that the optimization problem (14) does not include the disturbance  $\mathbf{w}(t)$ . The reason is that it is difficult to construct the  $M$ -step Lyapunov function in *Theorem 1* when the disturbance  $\mathbf{w}(t)$  is included, so that the robust stability of Dd-MHE cannot be deduced theoretically. In addition, if appropriate parameters can be determined, including the disturbance  $\mathbf{w}(t)$  will improve the performance of Dd-MHE and can cancel *Assumption 2* of this paper. It is an interesting issue to include the disturbance  $\mathbf{w}(t)$  and choose the appropriate parameters in the future.

*Remark 2:* In eddy current de-tumbling, the chaser stays close to the target for a long time. For example, the distance to the target surface is about 1 (m) [29]. However, the measurement of target's angular velocity based on LIDAR or optical encoder has been a difficult problem when the relative distance is short and the target rotates at high speed [30], [31]. Therefore, the historical data is obtained by LIDAR or optical encoder within their effective range. Then, Algorithm 1 is used to estimate the target's angular velocity when the distance is close and the target rotates at high speed. In addition, historical data that does not rely on ground truth angular velocity of the target are better, but this issue is still under study. In the latest research, Wolff et al. [32] solve the problem that the ground truth data contains noise but still relies on the ground truth historical data. We hope to solve the dependence of this algorithm on ground truth historical data in future research.

**B. Robust Stability**

In order to illustrate the robust stability of Dd-MHE, we introduce the time-discounted robust stability [25] of the following convolution sum form. Let  $\mathbf{e}(t) = \mathbf{x}(t) - \hat{\mathbf{x}}(t)$  and  $\bar{\mathbf{e}}(0) = \mathbf{x}(0) - \bar{\mathbf{x}}(0)$ , then we have the following definition.

*Definition 2:* (Def. 1 of [33], Def. 2.3 of [34]). A state estimator is robustly globally exponentially stable (RGES) if there exist  $\lambda_x, \lambda_w, \lambda_v \in (0, 1)$  and  $c_x, c_w, c_v > 0$ , such that the resulting state estimate  $\hat{\mathbf{x}}(t)$  satisfies

$$\|\mathbf{e}(t)\| \leq c_x \lambda_x^t \|\bar{\mathbf{e}}(0)\| + \sum_{j=0}^{t-1} c_w \lambda_w^{t-j-1} \|\mathbf{w}(j)\| + \sum_{j=0}^{t-1} c_v \lambda_v^{t-j-1} \|\mathbf{v}(j)\|, \quad (16)$$

for all  $t \in \mathbb{I}_{\geq 0}$ , all initial conditions  $\mathbf{x}(0), \bar{\mathbf{x}}(0) \in \mathbb{X}$ , and every system trajectory  $\{\mathbf{x}(t), \mathbf{y}(t), \mathbf{w}(t), \mathbf{v}(t)\}_{t=0}^{\infty}$ .

Note that the generalized definition of RGES is the convolution maximum form, that is,  $\|\mathbf{e}(t)\| \leq \beta_x(\|\bar{\mathbf{e}}(0)\|, t) \oplus \max_{j \in \mathbb{I}_{[0, t-1]}} \beta_w(\|\mathbf{w}(j)\|, t - j - 1) \oplus \max_{j \in \mathbb{I}_{[0, t-1]}} \beta_v(\|\mathbf{v}(j)\|, t - j - 1)$  with  $\beta_x, \beta_w, \beta_v \in \mathcal{KL}$ . However, the two forms are equivalent for the exponential stable case, given by Proposition 3.13 of [35]. Therefore, for simplicity, we directly use the above convolution sum form.

*Remark 3:* The definition of robust stability in the time-discounted form, also called as convolution maximization form in [34], is a new tool for dealing with the robust stability of more general estimators, which is discussed in detail in [25], [34], [35]. Compared with the asymptotic gain form, as in Def. 3 of [3], the robust stability of the time-discounted form can ensure that the robustness will not deteriorate with the increase of the horizon length, etc., as discussed in the abstract of [35].

To prove RGES, we give the following assumption as:

*Assumption 1:* The matrix pair  $(\mathbf{A}_{\bar{\mathbf{x}}}, \mathbf{C}_{\bar{\mathbf{x}}})$  of system (5) is observable.

Under this assumption, we have the following proposition:

*Proposition 1:* For any two trajectories of system (5),  $\{\mathbf{x}_1(t), \mathbf{y}_1(t), \mathbf{w}_1(t), \mathbf{v}_1(t), \mathbf{e}_1, \mathbf{r}_1\}$  and  $\{\mathbf{x}_2(t), \mathbf{y}_2(t), \mathbf{w}_2(t), \mathbf{v}_2(t), \mathbf{e}_2, \mathbf{r}_2\}$ , there exist  $\rho \in (0, 1)$  and  $\mu > 0$  such that

$$\|\mathbf{x}_\Delta(t+1)\|^2 \leq \rho \|\mathbf{x}_\Delta(t)\|^2 + \mu (\|\mathbf{y}_\Delta(t)\|^2 + \|\mathbf{r}_\Delta\|^2 + \|\mathbf{v}_\Delta(t)\|^2 + \|\mathbf{e}_\Delta\|^2 + \|\mathbf{w}_\Delta(t)\|^2), \quad (17)$$

where  $\mathbf{x}_\Delta(t) = \mathbf{x}_1(t) - \mathbf{x}_2(t)$ ,  $\mathbf{y}_\Delta(t) = \mathbf{y}_1(t) - \mathbf{y}_2(t)$ ,  $\mathbf{w}_\Delta(t) = \mathbf{w}_1(t) - \mathbf{w}_2(t)$ ,  $\mathbf{v}_\Delta(t) = \mathbf{v}_1(t) - \mathbf{v}_2(t)$ ,  $\mathbf{e}_\Delta = \mathbf{e}_1 - \mathbf{e}_2$ ,  $\mathbf{r}_\Delta = \mathbf{r}_1 - \mathbf{r}_2$ .

*Proof:* According to the superposition property of the system (5), we have

$$\mathbf{x}_\Delta(t+1) = \mathbf{A}_{\bar{\mathbf{x}}} \mathbf{x}_\Delta(t) + \mathbf{e}_\Delta + \mathbf{w}_\Delta(t), \quad (18)$$

$$\mathbf{y}_\Delta(t) = \mathbf{C}_{\bar{\mathbf{x}}} \mathbf{x}_\Delta(t) + \mathbf{r}_\Delta + \mathbf{v}_\Delta(t). \quad (19)$$

Thus, we can obtain the following equation by giving a matrix  $\mathbf{L}$ :

$$\mathbf{x}_\Delta(t+1) = \mathbf{A}_L \mathbf{x}_\Delta(t) + \mathbf{e}_\Delta + \mathbf{w}_\Delta(t) + \mathbf{L}(\mathbf{r}_\Delta + \mathbf{v}_\Delta(t) - \mathbf{y}_\Delta(t)), \quad (20)$$

where  $\mathbf{A}_L = \mathbf{A}_{\hat{\mathbf{x}}} + \mathbf{L}\mathbf{C}_{\hat{\mathbf{x}}}$ . Combining the above results with the Cauchy-Schwarz inequality,  $\mathbf{x}_\Delta(t+1)$  satisfies

$$\begin{aligned} \|\mathbf{x}_\Delta(t+1)\|^2 &\leq 6(\|\mathbf{A}_L\mathbf{x}_\Delta(t)\|^2 + \|\mathbf{e}_\Delta\|^2 + \|\mathbf{w}_\Delta(t)\|^2 \\ &\quad + \|\mathbf{L}\mathbf{y}_\Delta(t)\|^2 + \|\mathbf{L}\mathbf{r}_\Delta\|^2 + \|\mathbf{L}\mathbf{v}_\Delta(t)\|^2) \\ &\leq \rho\|\mathbf{x}_\Delta(t)\|^2 + \mu(\|\mathbf{y}_\Delta(t)\|^2 + \|\mathbf{r}_\Delta\|^2 \\ &\quad + \|\mathbf{v}_\Delta(t)\|^2 + \|\mathbf{e}_\Delta\|^2 + \|\mathbf{w}_\Delta(t)\|^2), \end{aligned} \quad (21)$$

where  $\mu$  and  $\rho$  are positive numbers satisfied the constraints:

$$6\lambda_{\max}(\mathbf{L}^\top\mathbf{L}) \leq \mu, \quad 6\lambda_{\max}(\mathbf{A}_L^\top\mathbf{A}_L) \leq \rho < 1. \quad (22)$$

Thus, (17) is derived.  $\blacksquare$

*Remark 4:* In the above proof, we require the parameters  $\mu$  and  $\rho$  to satisfy (22). However, since the system is unknown, the lower bound in (22) is also unknown. The **Algorithm 2** in Appendix I can calculate the parameters  $\rho_0$  and  $\mu_0$  that meet the constraints  $\rho_0 := 6\lambda_{\max}(\mathbf{A}_L^\top\mathbf{A}_L) \in (0, 1)$  and  $\mu_0 := 6\lambda_{\max}(\mathbf{L}^\top\mathbf{L})$ . Thus, (22) holds for  $\mu \geq \mu_0$  and  $1 > \rho \geq \rho_0$ .

To ensure the feasibility of the subsequent proof, we require the following assumption:

*Assumption 2:* For all  $t \in \mathbb{I}_{\geq 0}$ ,  $\mathbf{x}(t+1) - \mathbf{w}(t) \in \mathbb{X}$ .

This assumption is equivalent to  $\mathbf{A}_{\hat{\mathbf{x}}}\mathbf{x}(t) + \mathbf{e}_{\hat{\mathbf{x}}} \in \mathbb{X}$  and makes the state constraint satisfied for all  $\mathbf{x}(t)$  with  $t \in \mathbb{I}_{\geq 0}$ .

In what follows, we combine *Lemma 1* with **Theorem 1** of Ref. [27] to give the conclusion that  $W_\delta(\hat{\mathbf{x}}(t), \mathbf{x}(t)) = \|\mathbf{x}(t) - \hat{\mathbf{x}}(t)\|^2$  is the  $M$ -step Lyapunov function of Dd-MHE.

*Theorem 1:* ( $M$ -step Lyapunov function for data-driven MHE of Algorithm 1). Let Assumption 1 hold. Then, for all  $t \in \mathbb{I}_{\geq 0}$ , there exist  $\rho \in (0, 1)$  and  $\mu > 0$  such that the state estimate  $\hat{\mathbf{x}}$  by Algorithm 1 satisfies

$$\begin{aligned} \|\mathbf{x}(t) - \hat{\mathbf{x}}(t)\|^2 &\leq 4\rho^{M_t}\|\mathbf{x}(t - M_t) - \bar{\mathbf{x}}(t - M_t)\|^2 \\ &\quad + \sum_{j=1}^{M_t} \rho^{j-1} \mu (\|\mathbf{w}(t-j)\|^2 + 2\|\mathbf{v}(t-j)\|^2). \end{aligned} \quad (23)$$

*Proof:* The proof is divided into two parts. In the first part, we consider that the solution of Algorithm 1 is the trajectory of the system (5) and give the following inequality

$$\begin{aligned} \|\mathbf{x}(t) - \hat{\mathbf{x}}^*(t|t)\|^2 &\leq 2\rho^{M_t}\|\mathbf{x}(t - M_t) - \bar{\mathbf{x}}(t - M_t)\|^2 \\ &\quad + \sum_{j=1}^{M_t} \rho^{j-1} \mu (\|\mathbf{w}(t-j)\|^2 + \|\mathbf{v}(t-j)\|^2) \\ &\quad + J_L(\hat{\mathbf{x}}^*(t - M_t|t), \hat{\mathbf{v}}^*(\cdot|t), t). \end{aligned} \quad (24)$$

In the second part, we complete the proof of Theorem 1 by constructing a feasible solution to the optimization problem (14) and inequality (24).

**Part I:** Let the real trajectory of the system (5) be the first trajectory, i.e.,  $\mathbf{x}_1(t) = \mathbf{x}(t)$ ,  $\mathbf{y}_1(t) = \mathbf{y}(t)$ ,  $\mathbf{w}_1(t) = \mathbf{w}(t)$ ,  $\mathbf{v}_1(t) = \mathbf{v}(t)$ ,  $\mathbf{e}_1 = \mathbf{e}_{\hat{\mathbf{x}}}$ ,  $\mathbf{r}_1 = \mathbf{r}_{\hat{\mathbf{x}}}$ . In addition, according to *Lemma 1*,  $\hat{\mathbf{x}}_{[-M_t, 0]}^*(t)$  and  $\mathbf{y}_{[t-M_t, t-1]} - \hat{\mathbf{v}}_{[-M_t, -1]}^*(t)$  can be regarded as a trajectory of the system (5) without disturbance and noise. Thus, we have the second trajectory as  $\mathbf{x}_2(t-j) = \hat{\mathbf{x}}^*(t-j|t)$  with  $j \in \mathbb{I}_{[0, M_t]}$ , and  $\mathbf{y}_2(t-j) = \mathbf{y}(t-j) - \hat{\mathbf{v}}^*(t-j|t)$ ,  $\mathbf{w}_2(t-j) = \mathbf{0}$ ,  $\mathbf{v}_2(t-j) = \mathbf{0}$  with  $j \in \mathbb{I}_{[1, M_t]}$ , and  $\mathbf{e}_2 = \mathbf{e}_{\hat{\mathbf{x}}}$ ,  $\mathbf{r}_2 = \mathbf{r}_{\hat{\mathbf{x}}}$ .

Substituting the above two trajectories into Proposition 1, we get the following inequality as

$$\begin{aligned} \|\mathbf{e}^*(t|t)\|^2 &\leq \rho\|\mathbf{e}^*(t-1|t)\|^2 + \mu(\|\hat{\mathbf{v}}^*(t-1|t)\|^2 \\ &\quad + \|\mathbf{v}(t-1)\|^2 + \|\mathbf{w}(t-1)\|^2), \end{aligned} \quad (25a)$$

$$\begin{aligned} \|\mathbf{e}^*(t-1|t)\|^2 &\leq \rho\|\mathbf{e}^*(t-2|t)\|^2 + \mu(\|\hat{\mathbf{v}}^*(t-2|t)\|^2 \\ &\quad + \|\mathbf{v}(t-2)\|^2 + \|\mathbf{w}(t-2)\|^2), \end{aligned} \quad (25b)$$

$\vdots$

$$\begin{aligned} \|\mathbf{e}^*(t-M_t+1|t)\|^2 &\leq \rho\|\mathbf{e}^*(t-M_t|t)\|^2 + \mu(\|\hat{\mathbf{v}}^*(t-M_t|t)\|^2 \\ &\quad + \|\mathbf{v}(t-M_t)\|^2 + \|\mathbf{w}(t-M_t)\|^2), \end{aligned} \quad (25c)$$

where  $\mathbf{e}^*(t-j|t) = \mathbf{x}(t-j) - \hat{\mathbf{x}}^*(t-j|t)$ , for all  $j \in \mathbb{I}_{[0, M_t]}$ .

Substitute (25b) into (25a) and repeat this substitution for  $\|\mathbf{e}^*(t-2|t)\|^2, \|\mathbf{e}^*(t-3|t)\|^2, \dots, \|\mathbf{e}^*(t-M_t+1|t)\|^2$ , then

$$\begin{aligned} \|\mathbf{e}^*(t|t)\|^2 &\leq \rho^2\|\mathbf{e}^*(t-2|t)\|^2 \\ &\quad + \rho\mu(\|\hat{\mathbf{v}}^*(t-2|t)\|^2 + \|\mathbf{v}(t-2)\|^2 + \|\mathbf{w}(t-2)\|^2) \\ &\quad + \mu(\|\hat{\mathbf{v}}^*(t-1|t)\|^2 + \|\mathbf{v}(t-1)\|^2 + \|\mathbf{w}(t-1)\|^2) \\ &\leq \dots \leq \rho^{M_t}\|\mathbf{e}^*(t-M_t|t)\|^2 + \sum_{j=1}^{M_t} \rho^{j-1} \mu (\|\hat{\mathbf{v}}^*(t-j|t)\|^2 \\ &\quad + \|\mathbf{v}(t-j)\|^2 + \|\mathbf{w}(t-j)\|^2). \end{aligned} \quad (26)$$

Using the Cauchy-Schwarz inequality as

$$\begin{aligned} \|\mathbf{e}^*(t-M_t|t)\|^2 &\leq 2\|\bar{\mathbf{e}}(t-M_t)\|^2 \\ &\quad + 2\|\hat{\mathbf{x}}^*(t-M_t|t) - \bar{\mathbf{x}}(t-M_t)\|^2, \end{aligned} \quad (27)$$

where  $\bar{\mathbf{e}}(t-j) = \mathbf{x}(t-j) - \bar{\mathbf{x}}(t-j)$  for all  $j \in \mathbb{I}_{[1, M_t]}$ , we can continue the derivation to obtain that

$$\begin{aligned} \|\mathbf{e}^*(t|t)\|^2 &\stackrel{(27)}{\leq} 2\rho^{M_t}\|\bar{\mathbf{e}}(t-M_t)\|^2 \\ &\quad + \sum_{j=1}^{M_t} \rho^{j-1} \mu (\|\mathbf{w}(t-j)\|^2 + \|\mathbf{v}(t-j)\|^2) \\ &\quad + 2\rho^{M_t}\|\hat{\mathbf{x}}^*(t-M_t|t) - \bar{\mathbf{x}}(t-M_t)\|^2 \\ &\quad + \sum_{j=1}^{M_t} \rho^{j-1} \mu \|\hat{\mathbf{v}}^*(t-j|t)\|^2 \\ &\stackrel{(15)}{\leq} 2\rho^{M_t}\|\mathbf{x}(t-M_t) - \bar{\mathbf{x}}(t-M_t)\|^2 \\ &\quad + \sum_{j=1}^{M_t} \rho^{j-1} \mu (\|\mathbf{w}(t-j)\|^2 + \|\mathbf{v}(t-j)\|^2) \\ &\quad + J_L(\hat{\mathbf{x}}^*(t-M_t|t), \hat{\mathbf{v}}^*(\cdot|t), t). \end{aligned} \quad (28)$$

**Part II:** Consider a sequence of state/output data  $\mathbf{d}_t = \{\mathbf{x}(t-M_t), \mathbf{x}(t-M_t+1) - \mathbf{w}(t-M_t), \dots, \mathbf{x}(t) - \mathbf{w}(t-1)\}$ ,  $[\mathbf{y}(t-M_t) - \mathbf{v}(t-M_t), \dots, \mathbf{y}(t-1) - \mathbf{v}(t-1)]\}$ . It is obvious that  $\mathbf{d}_t$  is a disturbance-free and noise-free trajectory of the system (5) and satisfies (14a). Combined with Assumption 2, the data sequence  $\mathbf{d}_t$  is a feasible solution to the optimization problem (14). Thus, we have

$$J_L(\hat{\mathbf{x}}^*(t-M_t|t), \hat{\mathbf{v}}^*(\cdot|t), t) \leq J_L(\mathbf{x}(t-M_t), \mathbf{v}_{[t-M_t, t-1]}, t). \quad (29)$$

Substituting (29) into (28) yields that

$$\begin{aligned} \|e^*(t|t)\|^2 &\leq 2\rho^{M_t} \|\mathbf{x}(t - M_t) - \bar{\mathbf{x}}(t - M_t)\|^2 \\ &\quad + \sum_{j=1}^{M_t} \rho^{j-1} \mu (\|\mathbf{w}(t-j)\|^2 + \|\mathbf{v}(t-j)\|^2) \\ &\quad + J_L(\mathbf{x}(t - M_t), \mathbf{v}_{[t-M_t, t-1]}, t) \\ &= 4\rho^{M_t} \|\mathbf{x}(t - M_t) - \bar{\mathbf{x}}(t - M_t)\|^2 \\ &\quad + \sum_{j=1}^{M_t} \rho^{j-1} \mu (\|\mathbf{w}(t-j)\|^2 + 2\|\mathbf{v}(t-j)\|^2). \end{aligned} \quad (30)$$

It completes the proof.  $\blacksquare$

From the above proof, it is clear that the contraction property of the  $M$ -step Lyapunov function is satisfied by

$$\kappa^M = 4\rho^M < 1. \quad (31)$$

Note that since we assume observability, the robust stability of MHE still holds for  $\rho = 0$  and  $\kappa = 0$ . The interested reader is referred to Section 4.3.1 of [36] to complete the proof of robust stability for  $\rho = 0$  and  $\kappa = 0$ .

Finally, we give RGES of Dd-MHE based on  $M$ -step Lyapunov function as follows.

*Theorem 2:* Let Assumptions 1 and 2 hold, and the horizon length  $M$  satisfies (31). Then, for all  $t \in \mathbb{I}_{\geq 0}$ , the estimation error  $\mathbf{x}(t) - \hat{\mathbf{x}}(t)$  satisfies

$$\begin{aligned} \|\mathbf{x}(t) - \hat{\mathbf{x}}(t)\| &\leq (\sqrt{\kappa})^t \|\mathbf{x}(0) - \bar{\mathbf{x}}(0)\| \\ &\quad + \sum_{j=0}^{t-1} (\sqrt{\kappa})^{t-1-j} \sqrt{\mu} (\|\mathbf{w}(j)\| + \sqrt{2}\|\mathbf{v}(j)\|), \end{aligned} \quad (32)$$

with  $\kappa \in (0, 1)$  as defined in (31) and  $\rho, \mu$  in (21). Thus, Dd-MHE is RGES.

*Proof:* This proof has similar steps to the proof of Corollary 1 in [27]. We only list the key steps here.

Let  $t = kM + l$ , where  $l \in \mathbb{I}_{[1, M-1]}$  and  $k \in \mathbb{I}_{\geq 0}$ . Thus, when  $k = 0$ , we have  $l = M_t = t$ . Then, according to (30) and  $0 < \rho < \kappa$ , there is

$$\begin{aligned} \|e(l)\|^2 &= \|e^*(l|l)\|^2 \leq \kappa^l \|\mathbf{x}(0) - \bar{\mathbf{x}}(0)\|^2 \\ &\quad + \sum_{j=1}^l \kappa^{j-1} \mu (\|\mathbf{w}(l-j)\|^2 + 2\|\mathbf{v}(l-j)\|^2). \end{aligned} \quad (33)$$

For  $k \geq 1$ , we have  $M_t = M$ . Through (23), we can get

$$\begin{aligned} \|e(t)\|^2 &\leq \kappa^{kM} \|\mathbf{x}(l) - \bar{\mathbf{x}}(l)\|^2 \\ &\quad + \sum_{i=0}^{k-1} \kappa^{iM} \sum_{j=1}^M \kappa^{j-1} \mu (\|\mathbf{w}(t-iM-j)\|^2 \\ &\quad \quad \quad + 2\|\mathbf{v}(t-iM-j)\|^2). \end{aligned} \quad (34)$$

Substituting (31) and (33) into (34), the following equation

can be given

$$\begin{aligned} \|e(t)\|^2 &\leq \kappa^t \|\mathbf{x}(0) - \bar{\mathbf{x}}(0)\|^2 \\ &\quad + \sum_{j=1}^l \kappa^{kM+j-1} \mu (\|\mathbf{w}(t-kM-j)\|^2 + 2\|\mathbf{v}(t-kM-j)\|^2) \\ &\quad + \sum_{i=0}^{k-1} \sum_{j=1}^M \kappa^{iM+j-1} \mu (\|\mathbf{w}(t-iM-j)\|^2 + 2\|\mathbf{v}(t-iM-j)\|^2) \\ &= \kappa^t \|\mathbf{x}(0) - \bar{\mathbf{x}}(0)\|^2 + \sum_{q=0}^{t-1} \kappa^{t-1-q} \mu (\|\mathbf{w}(q)\|^2 + 2\|\mathbf{v}(q)\|^2). \end{aligned} \quad (35)$$

Combining (33) and (35), and using the fact that  $\sqrt{\sum_{i=1}^n a_i} \leq \sum_{i=1}^n \sqrt{a_i}$  for all  $a_i \geq 0$ , we obtain

$$\begin{aligned} \|e(t)\| &\leq (\sqrt{\kappa})^t \|\mathbf{x}(0) - \bar{\mathbf{x}}(0)\| \\ &\quad + \sum_{q=0}^{t-1} (\sqrt{\kappa})^{t-1-q} \sqrt{\mu} (\|\mathbf{w}(q)\| + \sqrt{2}\|\mathbf{v}(q)\|), \end{aligned} \quad (36)$$

where  $t \in \mathbb{I}_{\geq 0}$ .  $\blacksquare$

## IV. EXPERIMENT AND SIMULATION

In this section, we design an experimental system and a full 3 Degrees Of Freedom (3-DOF) rotational spacecraft dynamics simulation to verify **Algorithm 1** on the eddy current de-tumbling mission. The Data-driven Koopman MHE (Dd-KMHE) and Data-driven Error State Kalman Filter (Dd-ESKF) are used as a comparison. The basic structure of the Dd-KMHE is shown in the [17], where the Extended Dynamic Mode Decomposition (EDMD) algorithm based on thin plate spline radial basis functions was used to generate the lifted linear system [9]. The basic framework of the Dd-ESKF is consistent with Section II-B of [37], where the system model is given by *Theorem 1* of [21]. The whole experiment includes nominal experiments, disturbance and noise experiments. The physical parameters in the 3-DOF rotational dynamics simulation are consistent with [29].

### A. Eddy Current De-tumbling Experiment

1) *Experiment description:* As shown in Fig.1, the experimental system includes a 2-axis linear module, a NdFeB permanent magnet, a target rotation system, and a computer. The 2-axis linear module adjusts the relative distance between the NdFeB permanent magnet and the target. The NdFeB permanent magnet generates a magnetic field, and a Net F/T Transducer is mounted underneath it to measure the de-tumbling torque.

The target rotation system is also shown in Fig.1 where a metal target starts to rotate under the drive of the brushless motor. After reaching a certain rotation speed, the computer sends a command to disengage the electromagnetic clutch, and the target starts to rotate freely. During this period, an optical encoder measures the target's angular velocity and sends the target's angular velocity information to the computer through the data acquisition card. Moreover, a ceramic bearing is used to reduce the frictional force during the target rotation.

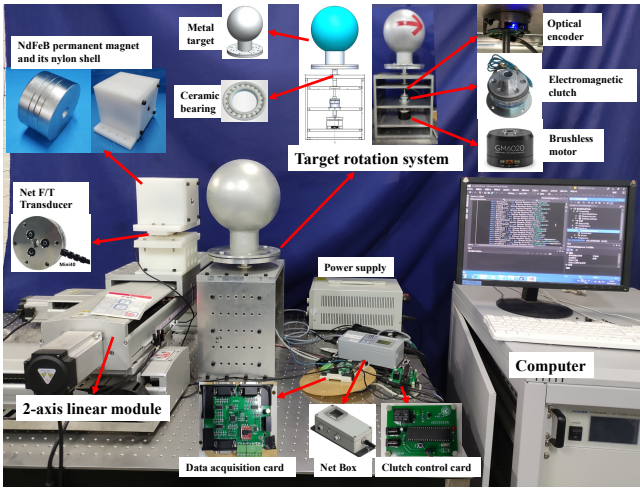


Fig. 1. Eddy current de-tumbling experimental system

The parameters of Dd-MHE in the experiment are  $\rho = 0.9$ ,  $M = 20$ ,  $\mu = 10^5$ . The constraint sets  $\mathbb{V} = \mathbb{R}$  and  $\mathbb{X} = \{\hat{\mathbf{x}}(t) | \mathbf{x} \leq \hat{\mathbf{x}}(t) - \mathbf{x}_c(t) \leq \bar{\mathbf{x}}\}$  where  $\mathbf{x}_c(t) = \mathbf{H}_{M_t+1}(\mathbf{x}_{[-T,0]})(\mathbf{H}_{M_t}(\mathbf{y}_{[-T,-1]}))^\dagger \mathbf{y}(t)$ ,  $\bar{\mathbf{x}} = -\mathbf{x} = \frac{10\pi}{60} \mathbf{1}_3$ . For comparison, Dd-KMHE adopts the same  $\rho$ ,  $M$ , and  $\mu$ , and the lifting dimension is set to 20. The center of the thin plate spline radial basis function is generated by random sequence. The sampling interval of data during the experiment is  $T_s = 0.01$  (s). The data in the first 0.5 (s), a total of 50 data, are used as historical data, so the estimated value in the first 0.5 (s) will be equal to the true value.

2) *Experimental results and analysis*: In this section, we show and analyze the results of the nominal experiment, the large sensor noise experiment, the large process disturbance experiment, and the experiment that contains both large noise and large disturbance.

Fig.2 shows that Dd-MHE, Dd-KMHE and Dd-ESKF converge for the nominal experiment. The parameters of Dd-ESKF are selected as  $Q = 0.9$  and  $R = 10^5$  to maintain the consistency of Dd-MHE. Such a choice of parameters means that Dd-ESKF will rely more on the system model than on the measured output. Therefore, Dd-ESKF exhibits strong noise robustness, but cannot track the state changes caused by disturbances, as shown in Fig.3 and Fig.4.

In the noise experiment (Fig.3), the estimation results of both Dd-MHE and Dd-KMHE show a bias, but both converge to the true value quickly after the noise ends. This bias is acceptable based on the fact that the estimators proposed in this paper are both data-driven. In addition, from Fig.3 to Fig.5, it can be found that Dd-MHE is more noise contaminated than that of the Dd-KMHE. It may be related to the fact that we only consider noise in the MHE optimization problem. As mentioned in *Remark 1*, the future focus will be on this issue.

The disturbance experiment (Fig.4) focuses on exploring the adaptability of the estimator to large process disturbances. Clearly, Dd-MHE shows significantly superior disturbance adaptation. It quickly tracks the true value after the disturbance. Dd-KMHE is less adaptive to the disturbance compared to Dd-MHE. In addition, we explored the estimator's perfor-

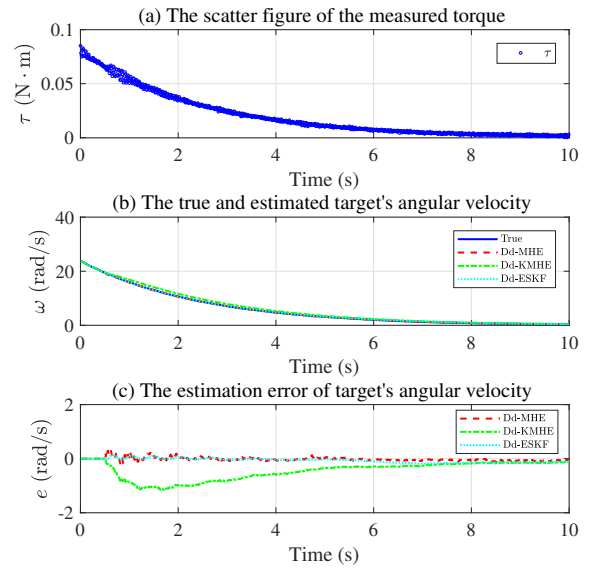


Fig. 2. Results of nominal estimation experiment.

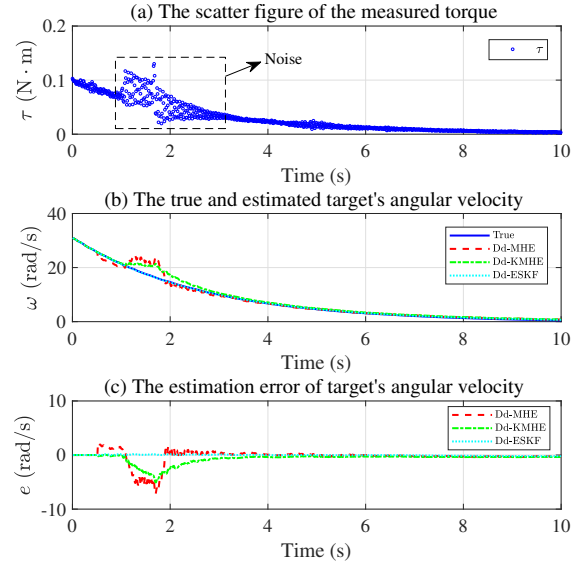


Fig. 3. Results of noise estimation experiment.

mance for the case of containing both noise and disturbances. As shown in Fig.5, Dd-KMHE exhibits unacceptably large deviations, while Dd-MHE exhibits good performance under complex perturbations and noise. The reason for the large performance difference is the lack of accuracy of the prediction model in Dd-KMHE due to the small amount of data.

Finally, we performed the sensitivity analysis for the parameter  $\mu$ . This parameter is essential for the performance and stability of the estimator. According to **Algorithm 2**,  $\rho_0 = 1.2705 \times 10^{-19}$ ,  $\mu_0 = 3.3307 \times 10^{-14}$ . Fig.6 shows the estimation results of Dd-MHE and Dd-KMHE for different values of  $\mu$ . Although the estimation results are stable for all  $\mu$ , Dd-KMHE is much more sensitive to  $\mu$ , while Dd-MHE is less affected by  $\mu$ . It means that when we do not know much about the system to be estimated, an unreasonable choice for  $\mu$  can lead to unacceptable bias in Dd-KMHE, while Dd-MHE

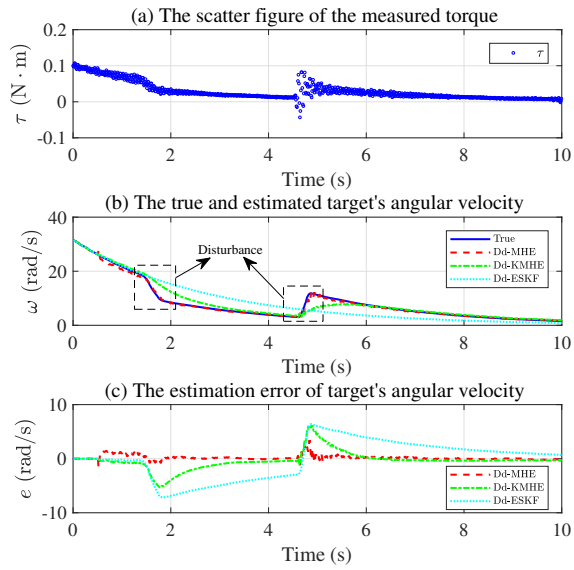


Fig. 4. Results of disturbance estimation experiment.

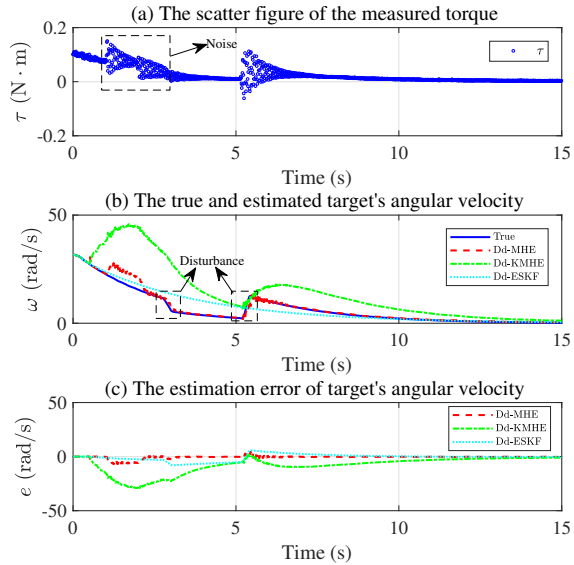


Fig. 5. Results of noise and disturbance estimation experiment.

tends to have a better estimation performance.

### B. 3-DOF rotational dynamics simulation

In this section, 3-DOF rotational dynamics simulation is adopted to demonstrate the performance of Dd-MHE for nonlinear systems. In this simulation, we employ the magnetic dipole approximation model for the de-tumbling torque, which is given as [19]:

$$\boldsymbol{\tau}_t(\boldsymbol{\omega}_t) = (\mathbf{M}_{\text{eff}}((\boldsymbol{\omega}_t - \boldsymbol{\omega}_c) \times \mathbf{B}_{Gt})) \times \mathbf{B}_{Gt}, \quad (37)$$

where  $\mathbf{M}_{\text{eff}}$  denotes the effective magnetic tensor, which is a constant matrix for a space target.  $\boldsymbol{\omega}_c$  denotes the angular velocity of the chaser, assumed to be constant.  $\mathbf{B}_{Gt}$  is the magnetic field at the center of gravity (COG) of the target. And the measurement output is

$$\boldsymbol{\tau}_c(\boldsymbol{\omega}_t) = -\boldsymbol{\tau}_t(\boldsymbol{\omega}_t) - \mathbf{r} \times \mathbf{F}_{ct}(\boldsymbol{\omega}_t), \quad (38)$$

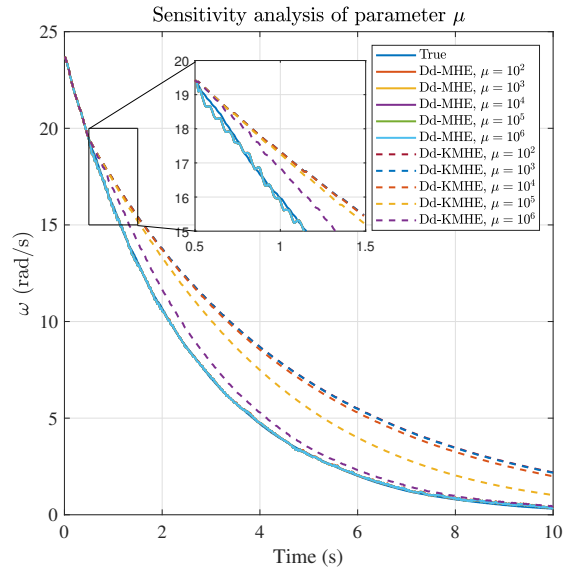


Fig. 6. Sensitivity analysis of parameter  $\mu$ .

where  $\mathbf{r}$  represents the relative position from the chaser to the target,  $\mathbf{F}_{ct}(\boldsymbol{\omega}_t)$  is the induced force on the target by the chaser given by

$$\mathbf{F}_{ct}(\boldsymbol{\omega}_t) = \boldsymbol{\Lambda}_{Gt} \mathbf{M}_{\text{eff}}((\boldsymbol{\omega}_t - \boldsymbol{\omega}_c) \times \mathbf{B}_{Gt}), \quad (39)$$

where  $\boldsymbol{\Lambda}_{Gt}$  is the Jacobian tensor of the magnetic field at the COG of the target. The above parameters in this simulation are taken as:  $\mathbf{J}_t = \text{diag}([4513.2, 4138.1, 3282.5])$  ( $\text{kg} \cdot \text{m}^2$ ),  $\mathbf{M}_{\text{eff}} = 0.89 \cdot 10^5 \cdot \text{diag}([5.908, 5.908, 1.951])$  ( $\text{S} \cdot \text{m}^4$ ),  $\boldsymbol{\omega}_c = \mathbf{0}$  ( $\text{deg/s}$ ),  $\boldsymbol{\omega}_t = [14.364, 1.224, 3.4195]^T$  ( $\text{deg/s}$ ),  $\mathbf{B}_{Gt} = [41, 51, -41]^T \cdot 10^{-4}$  (T),  $\mathbf{r} = [0.5, 1, 0.5]^T$  (m), and

$$\boldsymbol{\Lambda}_{Gt} = \begin{bmatrix} -23 & -116 & 8 \\ -116 & -119 & 49 \\ 8 & 49 & 142 \end{bmatrix} \cdot 10^{-4}.$$

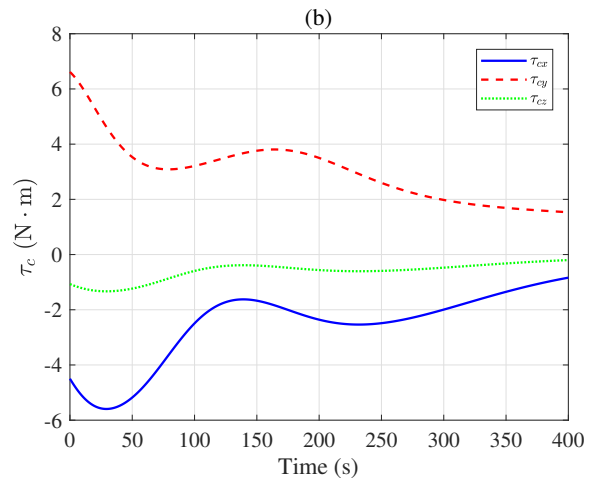


Fig. 7. Output of the simulation case

The parameters of Dd-MHE are:  $\rho = 0.8$ ,  $M = 10$ ,  $\mu = 10^5$  with  $\rho_0 = 0.4614$  and  $\mu_0 = 21.1561$ . The output of the simulation case is shown in Fig.7. In this simulation, we



assume that the measured values in the first 20 (s) are known and use them as historical data. After the 20 (s), the target's angular velocity can no longer be obtained directly, and the estimation of the target's angular velocity begins.

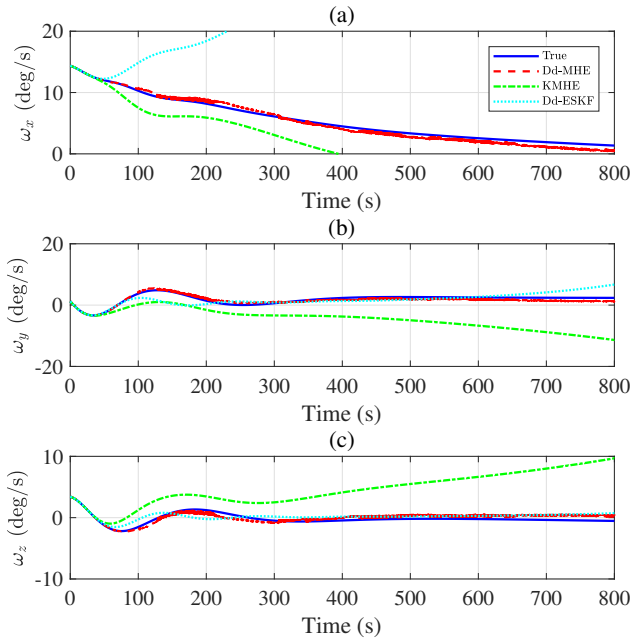


Fig. 8. The target's angular velocity and its estimation of 3-DOF rotational dynamics simulation

It can be seen from Fig.8 that Dd-MHE can well estimate the angular velocity of the target, but the performance of the Dd-KMHE and Dd-ESKF declines very fast. In the whole simulation, the estimated value by Dd-MHE is stable, while the estimated value by Dd-KMHE and Dd-ESKF is divergent. The reason for the estimated value by Dd-KMHE and Dd-ESKF diverging is that they both need a lot of data to obtain an accurate approximate model or appropriate parameters to reduce the dependence on the prediction model. In contrast, the Willem's fundamental lemma only needs to satisfy the rank condition (7). Therefore, Dd-MHE can estimate the angular velocity of the target well of a small data set.

## V. CONCLUSION

This paper proposes a data-driven moving horizon estimation method for small data sets and applies it to the angular velocity estimation of noncooperative targets in the eddy current de-tumbling mission. Compared with data-driven methods for large data sets or appropriate parameters, such as Dd-KMHE and Dd-ESKF, the proposed method in this paper has better estimation performance and is less sensitive to the parameter. However, since the method proposed in this paper is based on a local linear approximation, its effectiveness in strongly nonlinear systems is not yet known. It will be an issue that needs further study in the future.

## APPENDIX I POLE PLACEMENT FOR UNKNOWN SYSTEMS

The appendix is intended to provide a pole placement method for unknown systems. The method can give a state

observer gain  $L$  of unknown systems and make (22) hold.

### A. Dual system for Data-Driven Estimation

Consider the following unknown linear observable system

$$\mathbf{x}(t+1) = \mathbf{A}\mathbf{x}(t), \quad \mathbf{y}(t) = \mathbf{C}\mathbf{x}(t), \quad (40)$$

where  $\mathbf{x}(t) \in \mathbb{R}^n$  and  $\mathbf{y}(t) \in \mathbb{R}^p$  denote the system state and output at time  $t$ , respectively.  $\mathbf{A} \in \mathbb{R}^{n \times n}$  is the system matrix,  $\mathbf{C} \in \mathbb{R}^{p \times n}$  is the output matrix, and they are both unknown.  $n$  and  $p$  are the dimensions of the system state and output, respectively.

The dual system [38] for (40) is defined as

$$\mathbf{x}_{dl}(t+1) = \mathbf{A}^\top \mathbf{x}_{dl}(t) + \mathbf{C}^\top \mathbf{u}_{dl}(t), \quad (41)$$

where  $\mathbf{x}_{dl}(t) \in \mathbb{R}^n$  and  $\mathbf{u}_{dl}(t) \in \mathbb{R}^p$  denote the state and input of dual system at time  $t$ , respectively. Obviously, the observability of the original system (40) is equivalent to the controllability of the dual system (41). Then, our purpose is transformed into designing a controller gain matrix  $\mathbf{L}^\top$  of the dual system to satisfy (22). A detailed discussion of this idea can be found in [22].

Considering that the trajectory of the dual system will be used later, we give the following assumption and lemma.

*Assumption 3:* For a trajectory  $\{\mathbf{x}_{[0,T]}, \mathbf{y}_{[0,T-1]}\}$  of (40) with length  $T$ , and let  $\mathbf{X}_{0,T-1} = \mathbf{H}_1(\mathbf{x}_{[0,T-1]})$ ,  $\mathbf{X}_{1,T} = \mathbf{H}_1(\mathbf{x}_{[1,T]})$ ,  $\mathbf{Y}_{0,T-1} = \mathbf{H}_1(\mathbf{y}_{[0,T-1]})$ , it is assumed that  $\mathbf{X}_{0,T-1}$  and  $\begin{bmatrix} \mathbf{X}_{1,T} & \mathbf{Y}_{0,T-1} \end{bmatrix}$  have full rank, that is

$$\text{rank}(\mathbf{X}_{0,T-1}) = n, \quad \text{rank}\left(\begin{bmatrix} \mathbf{X}_{1,T} & \mathbf{Y}_{0,T-1} \end{bmatrix}\right) = n+p. \quad (42)$$

*Lemma 2:* [22] The data sequence

$$\mathbf{X}_{1,T}^{dl} = (\mathbf{X}_{0,T-1}^\top)^\dagger, \quad \begin{bmatrix} \mathbf{X}_{0,T-1}^{dl} \\ \mathbf{U}_{0,T-1}^{dl} \end{bmatrix} = \begin{bmatrix} \mathbf{X}_{1,T}^\top & \mathbf{Y}_{0,T-1}^\top \end{bmatrix}^\dagger, \quad (43)$$

is a trajectory of the dual system (41) in the meaning of least squares.

*Remark 5:* For the linear autonomous system with offsets such as (6), let

$$\mathbf{X}_{0,T-1} = \mathbf{H}_1(\mathbf{x}_{[1,T-1]}) - \mathbf{H}_1(\mathbf{x}_{[0,T-2]}), \quad (44a)$$

$$\mathbf{X}_{1,T} = \mathbf{H}_1(\mathbf{x}_{[2,T]}) - \mathbf{H}_1(\mathbf{x}_{[1,T-1]}), \quad (44b)$$

$$\mathbf{Y}_{0,T-1} = \mathbf{H}_1(\mathbf{y}_{[1,T-1]}) - \mathbf{H}_1(\mathbf{y}_{[0,T-2]}), \quad (44c)$$

then lemma 2 still holds under assumption 3.

### B. Pole Placement Method

In subsection Appendix I-A, we have transformed the pole placement for the state observer of the unknown system (40) into that for the controller of the dual system (41). The traditional pole placement method [38] includes a complex process, which is not conducive to unknown systems. In robust control, Linear Matrix Inequality (LMI) provides a convenient regional pole placement method [39]. In addition, the Linear Quadratic Regulation (LQR) of unknown systems are combined with LMI to ensure the controller's performance [21]. All these make LMI more suitable for dealing with the pole placement problem in this paper. Next, we briefly introduce the regional pole placement and data-driven LQR and give the pole placement method for unknown systems with guaranteed performance.

### 1) regional pole placement:

*Definition 3:* [39] A subset  $\mathcal{D}$  of the complex plane is called an LMI region if there exists a symmetric matrix  $\mathbf{L}_{\mathcal{D}}$  and a matrix  $\mathbf{M}_{\mathcal{D}}$  such that

$$\mathcal{D} = \{z \in \mathbb{C} : \mathbf{L}_{\mathcal{D}} + z\mathbf{M}_{\mathcal{D}} + z^*\mathbf{M}_{\mathcal{D}}^{\top} \prec 0\}, \quad (45)$$

where  $\mathbb{C}$  stands for the sets of complex numbers,  $z^*$  is the complex conjugate of  $z$ , “ $\prec$ ” denotes negative definite. Correspondingly, “ $\succ$ ” denotes positive definite.

Then, the following lemma gives the necessary and sufficient condition for the pole location in the LMI region  $\mathcal{D}$ .

*Lemma 3:* [39] The pole of matrix  $\mathbf{A}_L^{\top}$  is located in the LMI region  $\mathcal{D}$  if and only if there exists a symmetric positive definite matrix  $\mathbf{X}_{\mathcal{D}}$  such that

$$\mathbf{L}_{\mathcal{D}} \otimes \mathbf{X}_{\mathcal{D}} + \mathbf{M}_{\mathcal{D}} \otimes (\mathbf{A}_L^{\top} \mathbf{X}_{\mathcal{D}}) + \mathbf{M}_{\mathcal{D}}^{\top} \otimes (\mathbf{A}_L^{\top} \mathbf{X}_{\mathcal{D}})^{\top} \succ 0, \quad (46)$$

where  $\mathbf{A}_L^{\top} = \mathbf{A}^{\top} + \mathbf{C}^{\top} \mathbf{L}^{\top}$  is the system matrix of (41) with  $\mathbf{u}_{dl}(t) = \mathbf{L}^{\top} \mathbf{x}_{dl}(t)$ .

If the LMI region  $\mathcal{D}$  is a circle with radius  $r_{\mathcal{D}}$  centered at the origin, (46) can be converted to [39], [40]

$$\begin{bmatrix} -r_{\mathcal{D}} \mathbf{X}_{\mathcal{D}} & \mathbf{A}_L^{\top} \mathbf{X}_{\mathcal{D}} \\ (\mathbf{A}_L^{\top} \mathbf{X}_{\mathcal{D}})^{\top} & -r_{\mathcal{D}} \mathbf{X}_{\mathcal{D}} \end{bmatrix} \prec 0. \quad (47)$$

**2) data-driven LQR:** For the dual system (41), define the performance signal  $\mathbf{z}_{dl}(t)$  as

$$\mathbf{z}_{dl}(t) = \begin{bmatrix} \mathbf{Q}_{dl}^{1/2} & \mathbf{0} \\ \mathbf{0} & \mathbf{R}_{dl}^{1/2} \end{bmatrix} \begin{bmatrix} \mathbf{x}_{dl}(t) \\ \mathbf{u}_{dl}(t) \end{bmatrix}, \quad (48)$$

where  $\mathbf{Q}_{dl} = \mathbf{Q}_{dl}^{\top} \succ 0$ ,  $\mathbf{R}_{dl} = \mathbf{R}_{dl}^{\top} \succ 0$  are weighting matrices.

Thus, we have the data-driven LQR lemma as:

*Lemma 4:* [21] Let assumption 3 hold. Then, the data-driven LQR state-feedback gain  $\mathbf{L}^{\top}$  for system (41) can be computed as  $\mathbf{L}^{\top} = \mathbf{U}_{0,T-1}^{dl} \mathbf{X} (\mathbf{X}_{0,T-1}^{dl} \mathbf{X})^{-1}$  where  $\mathbf{X}$  optimizes

$$\min_{\mathbf{X}, \mathbf{W}} J = \text{Trace}(\mathbf{Q}_{dl} \mathbf{X}_{0,T-1}^{dl} \mathbf{X}) + \text{Trace}(\mathbf{W}), \quad (49a)$$

$$\text{s.t.} \begin{bmatrix} \mathbf{W} & \mathbf{R}_{dl}^{1/2} \mathbf{U}_{0,T-1}^{dl} \mathbf{X} \\ (\mathbf{U}_{0,T-1}^{dl} \mathbf{X})^{\top} \mathbf{R}_{dl}^{1/2} & \mathbf{X}_{0,T-1}^{dl} \mathbf{X} \end{bmatrix} \succ 0, \quad (49b)$$

$$\begin{bmatrix} \mathbf{X}_{0,T-1}^{dl} \mathbf{X} - \mathbf{I}_n & \mathbf{X}_{1,T}^{dl} \mathbf{X} \\ (\mathbf{X}_{1,T}^{dl} \mathbf{X})^{\top} & \mathbf{X}_{0,T-1}^{dl} \mathbf{X} \end{bmatrix} \succ 0. \quad (49c)$$

**3) Pole Placement for Unknown Systems:** Since  $\mathbf{A}_L^{\top}$  is unknown, (47) needs to be converted into data-driven form. Inspired by *Theorem 2* of [21], we have that  $\mathbf{A}_L^{\top} = \mathbf{X}_{1,T}^{dl} \mathbf{G}_L$  where  $\mathbf{G}_L$  is a  $T \times n$  matrix satisfying

$$\begin{bmatrix} \mathbf{L}^{\top} \\ \mathbf{I}_n \end{bmatrix} = \begin{bmatrix} \mathbf{U}_{0,T-1}^{dl} \\ \mathbf{X}_{0,T-1}^{dl} \end{bmatrix} \mathbf{G}_L. \quad (50)$$

Let  $\mathbf{X} = \mathbf{G}_L \mathbf{X}_{\mathcal{D}}$ , it is easy to deduce that

$$\mathbf{A}_L^{\top} = \mathbf{X}_{1,T}^{dl} \mathbf{X} \mathbf{X}_{\mathcal{D}}^{-1}, \quad \mathbf{X}_{\mathcal{D}} = \mathbf{X}_{0,T-1}^{dl} \mathbf{X}. \quad (51)$$

Thus, (47) can be converted to

$$\begin{bmatrix} -r_{\mathcal{D}} \mathbf{X}_{0,T-1}^{dl} \mathbf{X} & \mathbf{X}_{1,T}^{dl} \mathbf{X} \\ (\mathbf{X}_{1,T}^{dl} \mathbf{X})^{\top} & -r_{\mathcal{D}} \mathbf{X}_{0,T-1}^{dl} \mathbf{X} \end{bmatrix} \prec 0. \quad (52)$$

In addition, considering that  $\mathbf{X}_{\mathcal{D}}$  is a symmetric positive definite matrix, we give the following symmetric positive matrix constraints [41]:

$$\min_{\beta} \beta \quad (53a)$$

$$\text{s.t.} \begin{bmatrix} -\beta \mathbf{I}_n & \mathbf{X}_{0,T-1}^{dl} \mathbf{X} - \mathbf{X}^{\top} (\mathbf{X}_{0,T-1}^{dl})^{\top} \\ \star & -\mathbf{I}_n \end{bmatrix} \prec 0, \quad (53b)$$

$$\beta > 0, \quad \mathbf{X}_{0,T-1}^{dl} \mathbf{X} \succ 0, \quad (53c)$$

where  $\star$  is used to represent the symmetry of the matrix in (53b). The symmetric matrix constraints can be found in section 10.1 of [41].

To sum up, we give the following theorem to the observer pole placement for unknown systems.

*Theorem 3:* For the unknown linear observable system (40), let assumption 3 hold. Then, the observer pole is located in an LMI region  $\mathcal{D}$  with performance signal (48) if the observer gain  $\mathbf{L} = (\mathbf{U}_{0,T-1}^{dl} \mathbf{X} (\mathbf{X}_{0,T-1}^{dl} \mathbf{X})^{-1})^{\top}$  where  $\mathbf{X}$  optimizes

$$\min_{\mathbf{X}, \mathbf{W}, \beta} J = \text{Trace}(\mathbf{Q}_{dl} \mathbf{X}_{0,T-1}^{dl} \mathbf{X}) + \text{Trace}(\mathbf{W}) + \beta \quad (54a)$$

$$\text{s.t. (49b), (49c), (52), (53b) and (53c),} \quad (54b)$$

where  $\mathcal{D}$  is a circle with radius  $r_{\mathcal{D}}$  centered at the origin.

Finally, the following algorithm is given to make (22) satisfy.

---

**Algorithm 2:** Pole Placement for the unknown system (6) to make (22) satisfy.

---

**Data Preprocessing:** Given a trajectory of the system

(6) as  $\{\mathbf{x}_{[0,T]}, \mathbf{y}_{[0,T-1]}\}$ ; Given the initial guess  $\rho_0 \geq 1$  and  $r_{\mathcal{D}} < 1$ ; Given the symmetric weighting matrices  $\mathbf{Q}_{dl}$ ,  $\mathbf{R}_{dl}$ ; Define  $\mathbf{X}_{0,T-1}$ ,  $\mathbf{X}_{1,T}$ ,  $\mathbf{Y}_{0,T-1}$  as (44); Define  $\mathbf{X}_{0,T-1}^{dl}$ ,  $\mathbf{X}_{1,T}^{dl}$ ,  $\mathbf{U}_{0,T-1}^{dl}$  as (43).

**Numerical Iteration:**

**if** (42) holds **then**

**while**  $\rho_0 \geq 1$  **do**

        Solve equation (54) and obtain  $\mathbf{X}$ ;

        Let  $\rho_0 = 6\lambda_{\max}(\mathbf{A}_L^{\top} \mathbf{A}_L)$  and  $\mu_0 = 6\lambda_{\max}(\mathbf{L}^{\top} \mathbf{L})$  where  $\mathbf{A}_L^{\top}$  and  $\mathbf{L}$  are defined in (51) and *Theorem 3*, respectively.

**if**  $\rho_0 < 1$  **then**

            Return  $\rho_0$  and  $\mu_0$ . Break.

**else**

$r_{\mathcal{D}} = r_{\mathcal{D}}/2$ .

**end**

**end**

**else**

    The rank condition (42) is not satisfied. Break.

**end**

---

*Remark 6:* Algorithm 2 reduces the LMI region by setting  $r_{\mathcal{D}} = r_{\mathcal{D}}/2$ , however this is not unique. Other ways of reducing or adjusting  $r_{\mathcal{D}}$  are also feasible, such as  $r_{\mathcal{D}} = r_{\mathcal{D}} - a$  where  $a$  is a positive number. In addition, Algorithm 2 requires that the collected data come from system (6), that is, an offsets system without noise and disturbance. However, the actual data is derived from system (5) with noise and disturbance. It

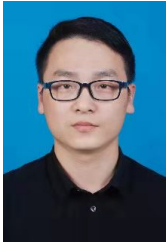
requires Algorithm 2 to be robust. One can select a smaller  $\rho_0$  or expand the LMI region  $\mathcal{D}$  into a robust LMI region [42].

## REFERENCES

- [1] X. Shao, Q. Hu, and Y. Shi, "Adaptive pose control for spacecraft proximity operations with prescribed performance under spatial motion constraints," *IEEE Transactions on Control Systems Technology*, vol. 29, no. 4, pp. 1405–1419, 2020.
- [2] X. Xia, E. Hashemi, L. Xiong, and A. Khajepour, "Autonomous vehicle kinematics and dynamics synthesis for sideslip angle estimation based on consensus kalman filter," *IEEE Transactions on Control Systems Technology*, 2022.
- [3] D. A. Allan and J. B. Rawlings, "Moving horizon estimation," in *Handbook of Model Predictive Control*. Springer, 2019, pp. 99–124.
- [4] Y. Zhang, P. Huang, Z. Meng, and Z. Liu, "Precise angles-only navigation for noncooperative proximity operation with application to tethered space robot," *IEEE Transactions on Control Systems Technology*, vol. 27, no. 3, pp. 1139–1150, 2018.
- [5] B. Gao, S. Gao, G. Hu, Y. Zhong, and C. Gu, "Maximum likelihood principle and moving horizon estimation based adaptive unscented kalman filter," *Aerospace Science and Technology*, vol. 73, pp. 184–196, 2018.
- [6] X. Liu, H. Chang, and P. Huang, "Eddy current de-tumbling large geostationary debris based on feedback linearization model predictive control," *Aerospace Science and Technology*, vol. 112, p. 106641, 2021.
- [7] Y. Liu, P. Huang, F. Zhang, and Y. Zhao, "Distributed formation control using artificial potentials and neural network for constrained multiagent systems," *IEEE Transactions on Control Systems Technology*, vol. 28, no. 2, pp. 697–704, 2018.
- [8] W.-H. Chen and F. You, "Semiclosed greenhouse climate control under uncertainty via machine learning and data-driven robust model predictive control," *IEEE Transactions on Control Systems Technology*, vol. 30, no. 3, pp. 1186–1197, 2021.
- [9] M. Korda and I. Mezić, "Linear predictors for nonlinear dynamical systems: Koopman operator meets model predictive control," *Automatica*, vol. 93, pp. 149–160, 2018.
- [10] L. Huang, J. Coulson, J. Lygeros, and F. Dörfler, "Decentralized data-enabled predictive control for power system oscillation damping," *IEEE Transactions on Control Systems Technology*, vol. 30, no. 3, pp. 1065–1077, 2021.
- [11] X.-B. Jin, R. J. Robert Jeremiah, T.-L. Su, Y.-T. Bai, and J.-L. Kong, "The new trend of state estimation: from model-driven to hybrid-driven methods," *Sensors*, vol. 21, no. 6, p. 2085, 2021.
- [12] Y. Weng, R. Negi, C. Faloutsos, and M. D. Ilić, "Robust data-driven state estimation for smart grid," *IEEE Transactions on Smart Grid*, vol. 8, no. 4, pp. 1956–1967, 2016.
- [13] Y. Chen, H. Chen, Y. Jiao, J. Ma, and Y. Lin, "Data-driven robust state estimation through off-line learning and on-line matching," *Journal of Modern Power Systems and Clean Energy*, vol. 9, no. 4, pp. 897–909, 2021.
- [14] S. L. Brunton and J. N. Kutz, *Data-driven science and engineering: Machine learning, dynamical systems, and control*. Cambridge University Press, 2022.
- [15] A. Surana and A. Banaszuk, "Linear observer synthesis for nonlinear systems using koopman operator framework," *IFAC-PapersOnLine*, vol. 49, no. 18, pp. 716–723, 2016.
- [16] A. Surana, M. O. Williams, M. Morari, and A. Banaszuk, "Koopman operator framework for constrained state estimation," in *2017 IEEE 56th Annual Conference on Decision and Control (CDC)*. IEEE, 2017, pp. 94–101.
- [17] A. Surana, "Koopman framework for nonlinear estimation," in *The Koopman Operator in Systems and Control*. Springer, 2020, pp. 59–79.
- [18] Z. C. Guo, V. Korotkine, J. R. Forbes, and T. D. Barfoot, "Koopman linearization for data-driven batch state estimation of control-affine systems," *IEEE Robotics and Automation Letters*, vol. 7, no. 2, pp. 866–873, 2021.
- [19] N. O. Gómez and S. J. Walker, "Guidance, navigation, and control for the eddy brake method," *Journal of Guidance, Control, and Dynamics*, vol. 40, no. 1, pp. 52–68, 2017.
- [20] J. C. Willems, P. Rapisarda, I. Markovsky, and B. L. De Moor, "A note on persistency of excitation," *Systems & Control Letters*, vol. 54, no. 4, pp. 325–329, 2005.
- [21] C. De Persis and P. Tesi, "Formulas for data-driven control: Stabilization, optimality, and robustness," *IEEE Transactions on Automatic Control*, vol. 65, no. 3, pp. 909–924, 2019.
- [22] R. Adachi and Y. Wakasa, "Dual system representation and prediction method for data-driven estimation," in *2021 60th Annual Conference of the Society of Instrument and Control Engineers of Japan (SICE)*. IEEE, 2021, pp. 1245–1250.
- [23] M. S. Turan and G. Ferrari-Trecate, "Data-driven unknown-input observers and state estimation," *IEEE Control Systems Letters*, vol. 6, pp. 1424–1429, 2021.
- [24] T. M. Wolff, V. G. Lopez, and M. A. Müller, "Data-based moving horizon estimation for linear discrete-time systems," *arXiv preprint arXiv:2111.04979*, 2021.
- [25] S. Knüfer and M. A. Müller, "Time-discounted incremental input/output-to-state stability," in *2020 59th IEEE Conference on Decision and Control (CDC)*. IEEE, 2020, pp. 5394–5400.
- [26] J. Berberich, J. Köhler, M. A. Müller, and F. Allgower, "Linear tracking lmg for nonlinear systems part ii: The data-driven case," *IEEE Transactions on Automatic Control*, 2022.
- [27] J. D. Schiller, S. Muntwiler, J. Köhler, M. N. Zeilinger, and M. A. Müller, "A lyapunov function for robust stability of moving horizon estimation," *arXiv preprint arXiv:2202.12744*, 2022.
- [28] L. P. Cassinis, R. Fonod, and E. Gill, "Review of the robustness and applicability of monocular pose estimation systems for relative navigation with an uncooperative spacecraft," *Progress in Aerospace Sciences*, vol. 110, p. 100548, 2019.
- [29] X. Liu, H. Chang, P. Huang, and Z. Lu, "Robust output-feedback predictive control for proximity eddy current de-tumbling with constraints and uncertainty," *IEEE Transactions on Aerospace and Electronic Systems*, 2022.
- [30] Q. Feng, Z. H. Zhu, Q. Pan, and Y. Liu, "Pose and motion estimation of unknown tumbling spacecraft using stereoscopic vision," *Advances in Space Research*, vol. 62, no. 2, pp. 359–369, 2018.
- [31] Y. Zhang, J. Xu, P. Zhang, W. Li, K. Yu, and P. Huang, "Monocular visual-inertial sensing of unknown rotating objects: Observability analyses and case study for metric 3d reconstructing of space debris," *IEEE Robotics and Automation Letters*, 2022.
- [32] T. M. Wolff, V. G. Lopez, and M. A. Müller, "Robust data-driven moving horizon estimation for linear discrete-time systems," *arXiv preprint arXiv:2210.09017*, 2022.
- [33] S. Knüfer and M. A. Müller, "Robust global exponential stability for moving horizon estimation," in *2018 IEEE Conference on Decision and Control (CDC)*. IEEE, 2018, pp. 3477–3482.
- [34] D. A. Allan, J. Rawlings, and A. R. Teel, "Nonlinear detectability and incremental input/output-to-state stability," *SIAM Journal on Control and Optimization*, vol. 59, no. 4, pp. 3017–3039, 2021.
- [35] D. A. Allan and J. B. Rawlings, "Robust stability of full information estimation," *SIAM Journal on Control and Optimization*, vol. 59, no. 5, pp. 3472–3497, 2021.
- [36] J. B. Rawlings, D. Q. Mayne, and M. Diehl, *Model predictive control: theory, computation, and design*. Nob Hill Publishing Madison, WI, 2017, vol. 2.
- [37] V. Madyastha, V. Ravindra, S. Mallikarjunan, and A. Goyal, "Extended kalman filter vs. error state kalman filter for aircraft attitude estimation," in *AIAA Guidance, Navigation, and Control Conference*, 2011, p. 6615.
- [38] F. M. Callier and C. A. Desoer, *Linear system theory*. Springer Science & Business Media, 1991.
- [39] M. Chilali and P. Gahinet, "H/sub/spl infin//design with pole placement constraints: an lmi approach," *IEEE Transactions on automatic control*, vol. 41, no. 3, pp. 358–367, 1996.
- [40] V. Wisniewski, E. Maddalena, and R. Godoy, "Discrete-time regional pole-placement using convex approximations: Theory and application to a boost converter," *Control Engineering Practice*, vol. 91, p. 104102, 2019.
- [41] E.-K. Boukas, *Control of singular systems with random abrupt changes*. Springer Science & Business Media, 2008.
- [42] M. Hypiusová and D. Rosinová, "Robust pole placement: D r-regions for discrete-time systems," in *2019 22nd International Conference on Process Control (PC19)*. IEEE, 2019, pp. 108–113.



**Xiyao Liu** (S'22) received the B.S. degree from Southwest Jiaotong University, Chengdu, China, in 2016. He is currently working toward the Ph.D. degree in navigation, guidance and control at the School of Astronautics, Northwestern Polytechnical University, Xi'an, China. His research focuses on model predictive control, data driven control, moving horizon estimation, and eddy current detumbling.



**Haitao Chang** (M'22) received B.S., M.S. and Ph.D. in navigation, guidance and control from Northwestern Polytechnical University, Xi'an China in 2010, 2013 and 2018 respectively. He is currently an assistant research professor with the School of Astronautics, Northwestern Polytechnical University. His research interests include space robot and control, space teleoperation, and space debris removal, etc.



**Zhenyu Lu** (M'21) received the Ph.D degree in Northwestern Polytechnical University, Xi'an, China in 2019. He is currently working as a senior research fellow in Bristol Robotic Laboratory & University of the West of England, Bristol. His research interests include teleoperation, human robotics interaction and intelligent learning method.



**Panfeng Huang** (S'01, M'05, SM'17) received the B.S. degree in test and measurement technology and the M.S. degree in navigation guidance and control from Northwestern Polytechnical University, Xi'an, China, in 1998 and 2001, respectively, and the Ph.D. degree in automation and robotics from The Chinese University of Hong Kong, Hong Kong, in 2005. He is currently a Professor with the School of Astronautics, Northwestern Polytechnical University, and the National Key Laboratory of Aerospace Flight Dynamics, and the Director of the Research Center for Intelligent Robotics, Northwestern Polytechnical University. His current research interests include tethered space robotics, intelligent control, machine vision, and space debris removal.

His current research interests include tethered space robotics, intelligent control, machine vision, and space debris removal.